Airway surface liquid depth imaged by surface laser reflectance microscopy

Jay R. Thiagarajah, Yuanlin Song, Nico Derichs, and A.S. Verkman

Department of Medicine and Department of Physiology, University of California, San Francisco, San Francisco, CA 94143

The thin layer of liquid at the surface of airway epithelium, the airway surface liquid (ASL), is important in normal airway physiology and in the pathophysiology of cystic fibrosis. At present, the best method to measure ASL depth involves scanning confocal microscopy after staining with an aqueous-phase fluorescent dye. We describe here a simple, noninvasive imaging method to measure ASL depth by reflectance imaging of an epithelial mucosa in which the surface is illuminated at a 45-degree angle by an elongated 13-µm wide rectangular beam produced by a 670-nm micro-focus laser. The principle of the method is that air–liquid, liquid–liquid, and liquid–cell interfaces produce distinct specular or diffuse reflections that can be imaged to give a micron-resolution replica of the mucosal surface. The method was validated using fluid layers of specified thicknesses and applied to measure ASL depth in cell cultures and ex vivo fragments of pig trachea. In addition, the method was adapted to measure transepithelial fluid transport from the dynamics of fluid layer depth. Compared with confocal imaging, ASL depth measurement by surface laser reflectance microscopy does not require dye staining or costly instrumentation, and can potentially be adapted for in vivo measurements using fiberoptics.

INTRODUCTION

The airway surface liquid (ASL) is the thin layer of aqueous fluid and mucus covering the airway surface at the interface between surface epithelial cells and the air space. The properties of the ASL, including its thickness ("depth"), composition, and rheology, facilitate mucociliary clearance, bacterial killing, and epithelial cell homeostasis (Blouquit-Laye and Chinet, 2007). Alterations in ASL depth likely contribute to cystic fibrosis (CF) lung disease (Verkman et al., 2003; Boucher, 2007) and perhaps to asthma and other pulmonary diseases (Boucher, 2004; Nakagami et al., 2008). Because of its importance in mucociliary clearance and consequent pathogenic bacterial colonization in CF, ASL depth has been proposed as a potential outcome measure for ion channel–targeted CF therapies, such as correctors of mutant CFTRs and inhibitors of epithelial sodium channels (Thelin and Boucher, 2007; Kreindler, 2010).

Measurement of ASL depth is technically challenging because it can be as low as 5–15 µm. Various methods have been used to estimate ASL depth, including electron microscopy of fixed frozen tissues or cells (Yager et al., 1994; Wu et al., 1996), microelectrode scanning (Rahmoune and Shephard, 1995), and z-scanning confocal microscopy (Jayaraman et al., 2001; Tarran et al., 2001; Song et al., 2009). Confocal fluorescence microscopy is at present probably the most reliable method to measure ASL depth. The ASL is stained with an aqueous-

phase fluorescent dye, then generally covered with oil (to prevent evaporation), and imaged by z-scanning confocal microscopy to reconstruct ASL depth profiles. Until recently, ASL depth measurements were done exclusively on airway cell cultures in which scanning is done with an immersion objective lens through a transparent porous filter supporting the epithelial cell layer. We recently introduced a modification of the scanning confocal microscopy method in which scanning is done from the mucosal side using an upright confocal microscope and water-immersion objective lens immersed in refractive index-matched perfluorocarbon covering the fluorescently stained ASL (Song et al., 2009). In that study, we also introduced an analysis method for quantitative computation of z-depths based on the z-point spread function of the microscope objective, using information from the entire image stack. Scanning from the mucosal side also allowed ASL depth measurements to be made in ex vivo airway tissue fragments.

Technical limitations of ASL depth measurement by scanning confocal fluorescence microscopy include the need to stain the ASL by dyes and to cover the aqueous ASL with nonaqueous fluid, such as oil or perfluorocarbon. Also, the acquisition of many z-scans for image reconstruction precludes measurement of rapid changes in ASL depth. ASL depth measurement by confocal microscopy requires costly instrumentation and custom

The Rockefeller University Press $30.00
J. Gen. Physiol. Vol. 136 No. 3   353–362
www.jgp.org/cgi/doi/10.1085/jgp.201010490

353

cell chambers, so that at present ASL depth measurements are made in only a few laboratories worldwide. Finally, it is not practical to adapt scanning confocal fluorescence microscopy for ASL studies in vivo.

To address these limitations, we introduce here a surface laser reflectance microscopy (SLRM) method to measure ASL depth. As diagrammed in Fig. 1 (A and B), the SLRM method relies on reflections of laser light from interfaces in the unstained mucosa, including the air–ASL interface and the ASL–cell interface. The largely specular reflection from the air–ASL interface and the largely diffuse reflection from the ASL–cell interface are imaged to reconstruct a replica of the mucosal surface. The method is implemented herein, validated in test systems, and applied to measure ASL depth and transepithelial fluid transport.

MATERIALS AND METHODS

Surface laser reflectance microscope

Surface reflectance measurements were made using the apparatus diagrammed in Fig. 1 C, which was assembled on a vibration isolation table (Newport Corporation). An MFL diode laser (660 nm, 5 mW; Edmund Optics) was held at an angle of 45 degrees using a micromanipulator. The diode laser produces a 10 mm × 13 µm line at a working distance of 65 mm. The incident laser beam was displaced using a glass prism to scan across 12-mm diameter circular cell culture inserts having 5-mm length side walls. Samples were placed on an xyz stage with 2-µm step displacement. Reflected light was captured by a stereozoom microscope (SMZ1500; Nikon) using a 1× objective (total magnification, 5–10×), which was held at an angle of 45 degrees. Images (1,600 × 1,200 pixels) were captured using a color CMOS camera (PL-A622C; PixeLINK).

Solution validation studies and depth profile analysis

In one set of studies, fluid volumes (5–20 µl) were deposited between square glass coverslips (22 × 22 mm; No. 1; Thermo Fisher Scientific) to produce specified fluid layer thicknesses. In another set of studies, specified volumes of PBS, mineral oil (type light oil; refractive index, 1.467; Sigma-Aldrich), and perfluorocarbon (FC-70; boiling point, 215°C; refractive index, 1.303; density, 1.9 g/ml; 3M), alone or in combination, were deposited on Snapwell tissue culture inserts (Corning), and reflectance images were recorded. Fluid layer thicknesses were measured in parallel by scanning confocal microscopy. Cover glass and fluid thicknesses were computed from intensity profiles perpendicular to reflections of the laser line (Fig. 1 D). Intensity profiles $I(x)$ at each reflection interface were fitted to a Gaussian function:

$$I(x) = A \, exp \, \{-(x - x_0)^2 / \sigma^2\}, \tag{1}$$

where A is the amplitude, x_0 is the position of the peak center, and σ^2 is the variance. The location of the interface, ε_n, was defined as the lower boundary of the 95% confidence interval:

$$\varepsilon_n = x_o - 3\sigma. \tag{2}$$

The distance, D_m, between interfaces was calculated from the difference in ε_n:

$$D_m = \varepsilon_{n+1} - \varepsilon_n, \tag{3}$$

where ε_n is the position of the nth interface. Absolute distances between interfaces were calculated taking into account the angle of incident light and the refractive indices of the various media (derived from Snell's Law):

$$n_1 \, sin \, \theta_1 = n_2 \, sin \, \theta_2, \tag{4}$$

where n_1 and n_2 are the refractive indices of each layer, and θ_1 and θ_2 are the angles from the normal of the incident and refracted
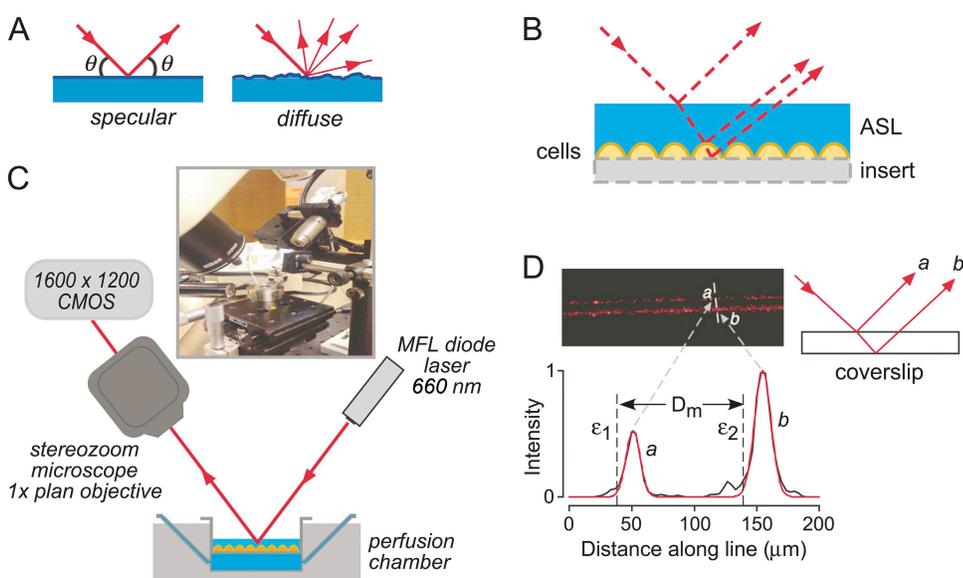
Figure 1. Principle and instrumentation for ASL depth measurement by SLRM. (A) Schematic showing light paths for diffuse versus specular laser reflections. (B) Schematic of incident, reflected, and refracted light paths for a fluid layer overlying cells on a culture insert, showing displacements of reflections from interfaces. (C) Diagram and photograph of SLRM apparatus. (D) Image of laser reflections from a cover glass (thickness, 0.1 mm; air–glass interface) (top left) with schematic showing origin of reflections a and b (top right). Intensity versus distance profile shown in black (bottom) with fitted Gaussian curves (red) at each interface. ε_1 and ε_2 are calculated locations of interfaces, and D_m is the distance between interfaces (cover glass thickness).

waves, respectively. For an air–liquid interface, $\theta_2 = arcsin\ (sin\ \theta_1\ /n_2)$, giving absolute distance $D_a = D_m\ cos\ \theta_2$.

Confocal microscopy
Scanning confocal microscopy was done as described previously (Song et al., 2009). The ASL was imaged using a confocal microscope (EZ-C1; Nikon) equipped with a water-immersion objective lens (40×; numerical aperture, 0.8; working distance, 2 mm; Plan APO; Nikon). Generally, a stack of 40–80 images (0.56–1-µm apart) was acquired over 40–60 s. The x-y–scanned area was 236 × 236 µm at a resolution of 256 × 256 pixels. The ASL was covered with FC-70 perfluorocarbon for immersion of the objective lens. The ASL was stained red with the aqueous-phase dye rhodamine B-dextran (40 kD; Invitrogen), and the epithelial cell cytoplasm was stained green with the cell-trappable dye CellTrace (Invitrogen). ASL depth was calculated from z-image stacks as described previously (Song et al., 2009).

Cell lines and culture
Primary cultures of human bronchial epithelial (HBE) cells were grown as described previously (Song et al., 2009). Cell number and viability (>90%) were determined by Trypan blue staining. Cells were plated at a density of 5×10^5 per cm^2 onto 12-mm diameter, 0.4-µm pore polycarbonate cell culture inserts (Snapwell; Corning) precoated with human placental collagen (15 mg/cm^2; Sigma-Aldrich). Cultures were grown at an air–liquid interface in ALI medium at 37°C, 5% CO_2/95% air, to develop functionally differentiated cell sheets. Medium was changed every 2–3 d. Cultures were used 21–35 d after plating, at which time transepithelial resistance was 400–1,000 Ω/cm^2 and a thin ASL film was seen. For some studies, T84 cells (American Type Culture Collection no. CCL-248) were plated onto cell culture inserts and grown for 10 d (transepithelial resistance, 1,000–1,300 Ω/cm^2).

ASL depth measurements in bronchial cell cultures
ASL depth in unperturbed well-differentiated bronchial cell cultures (days 21–35) was measured by SLRM, in which culture inserts were placed in a perfusion chamber containing warmed PBS with 10 mM glucose, which was maintained at 37°C using a perfusion chamber incubator (Harvard Apparatus). Measurements were done in <2 min to minimize evaporative effects. The mucosal surface was then washed with PBS, and cell cytoplasm was stained green by incubation for 10 min with 10 µM CellTrace (Invitrogen) in 100 µl PBS added onto the surface. Excess fluid was then removed from the insert, and cells were stained with rhodamine B-dextran (10 mg/ml; 40 kD) by depositing a small volume (20 µl) on top of the cells as described previously (Song et al., 2009). After 6–8 h, the airway cells absorbed most of the added fluid and a steady-state ASL thickness was achieved. Inserts were then placed in perfusion chambers maintained at 37°C, and ASL depth was measured by SLRM, and then in the same inserts by z-scanning confocal microscopy. For fluid absorption experiments in bronchial cell cultures, 20 µl of PBS containing 10 mM glucose and rhodamine B-dextran (10 mg/ml; 40 kD) was added to the mucosal surface, and ASL depth was measured at specified times by SLRM and confocal microscopy. In some experiments 100 µM amiloride was added to the PBS solution added on the mucosal surface.

Pig airways
Pig airways were obtained from Pork Farm. Fragments of airway mucosa taken from the posterior tracheal surface were mounted in perfusion chambers as described previously (Song et al., 2009). After incubation at 37°C for 45 min, the surface fluid was carefully removed using a pipette, and the mucosal surface was rinsed twice with PBS and dried briefly with an air stream. 20 µl of PBS containing rhodamine B-dextran (10 mg/ml; 40 kD) was added to the mucosal surface, which was then covered with 50 µl FC-70. ASL depth was measured by SLRM and z-scanning confocal microscopy just after FC-70 addition and at specified times thereafter. Between measurements, the perfusion chamber was maintained at 37°C in an incubator. For secretion measurements, 20 µM forskolin plus 100 µM 3-isobutyl-1-methylxanthine (IBMX) plus 1 mM carbachol (Sigma-Aldrich) was added to the perfusate, and ASL depth was measured by SLRM at specified times.

Transepithelial water permeability
For measurements of transepithelial water permeability, cells grown on cell culture inserts were placed in a perfusion chamber maintained at 37°C. 200 µl PBS was added to the mucosal (apical) surface. The basolateral perfusate solution was rapidly changed from isosmolar PBS to a hyperosmolar PBS solution containing 300 mM mannitol. SLRM images were taken at specified times. For reversal of the osmotic gradient, the basolateral PBS solution was maintained and 100 µl PBS containing 300 mM mannitol was added to the apical surface. Transepithelial osmotic water permeability coefficient (P_f; in cm/s) was computed from the rate of fluid volume change over the first 10 min (dV(0)/dt) by linear regression, from: $dV(0)/dt = P_f \cdot S \cdot v_w \cdot (\Phi_1 - \Phi_2)$, where S is the tissue surface area assuming a smooth surface (1.13 cm^2), v_w is the partial molar volume of water (18 cm^3/mol), and ($\Phi_1 - \Phi_2$) is the transepithelial osmotic gradient (3×10^{-4} mol/cm^3).

Data analysis and statistics
Laser reflectance images were analyzed using ImageJ (W. Rasband, National Institutes of Health, Bethesda, MD), and curve fitting and graphing of intensity profiles were done using Igor Pro (WaveMetrics, Inc.). Cell culture and pig trachea data were statistically analyzed using ANOVA with Tukey-Kramer post-hoc test for comparison between individual experimental groups.

RESULTS

SLRM instrument design and performance
Determination of ASL depth by SLRM relies on the reflections of incident light as it passes through interfaces of differing composition and/or refractive index. As diagrammed in Fig. 1 A, light reflection from a surface interface is specular or diffuse depending on the nature of the surface. Fig. 1 B shows that air–liquid and liquid–cell interfaces each reflect a portion of the incident light. The proportion of light that is reflected versus refracted depends on the angle of incident light and media refractive indices. Reflections from interfaces at different depths (z) are displaced with respect to each other, allowing computation of the absolute distance between interfaces.

To create appropriate reflections and measure the resultant displacements, an apparatus was assembled based on imaging of a sample that was illuminated by a narrow, line-shaped beam (13-µm wide and 10-mm long) produced by a 660-nm micro-focus laser diode held at a 45-degree angle (Fig. 1 C). A line-shaped laser beam rather than single laser spot was used to image reflections across the length of the line, allowing visualization of multiple reflection displacement points and hence the reconstruction of a replica-like ASL profile. A line-shape beam profile is also less susceptible to noise

from stray reflections or scattering within fluid layers. To measure ASL thickness in biological specimens, cell culture inserts or tissue fragments were placed in a custom-built perfusion chamber on an xyz stage, which allowed fine adjustment of laser line focus and movement of the beam across the sample. Reflected light was captured and focused using a stereozoom microscope tilted at an angle of 45 degrees and imaged using a digital camera. Fig. 1 D shows an example of an image from a cover glass showing laser line reflections coming from the top and bottom of the cover glass (labeled *a* and *b*). Also shown is the associated intensity versus distance profile measured perpendicular to the reflected laser lines. The profile shows the fitted intensity curves for each reflection, and the dashed lines at positions ε_1 and ε_2 indicate calculated interface positions. The displacement (D_m) between positions ε_1 and ε_2 is equal to the thickness of the cover glass.

To validate thickness determination by SLRM, measurements were made on specified fluid layer thicknesses in which known fluid volumes were sandwiched between glass coverslips. Fig. 2 A shows greater displacements of the laser line reflections with increasing fluid thickness. Fig. 2 B (left) shows increasing distance between the corresponding peaks in the intensity versus

distance profiles, with an expanded view of the profiles of the second reflections shown in Fig. 2 B (middle). Fluid layer thicknesses computed from SLRM were in agreement with those specified from the amount of added fluid (Fig. 2 B, right). The resolution for determination of fluid layer thickness by SLRM was assessed by serial measurements of reflectance from a single interface with small (2-µm) step displacements of the sample perpendicular to the laser line in the z-direction. Fig. 2 C (left) shows intensity versus distance profiles, and Fig. 2 C (right) shows agreement between actual and computed displacements, indicating a resolution of 1 µm or better. Fig. 2 D verifies that the ability of SLRM to determine layer thickness is independent of incident angle. A 100-µm-thick cover glass was imaged at different incident angles. Fig. 2 D shows the expected increase in measured width (in pixel units) with reduced incident angle, which was in agreement with the width predicted from the incident angle and refractive index of glass.

Fluid layer thickness measured by SLRM

Measurement of ASL thickness in epithelial cell cultures requires cell growth on porous filters for cell polarization and creation of high-resistance intercellular
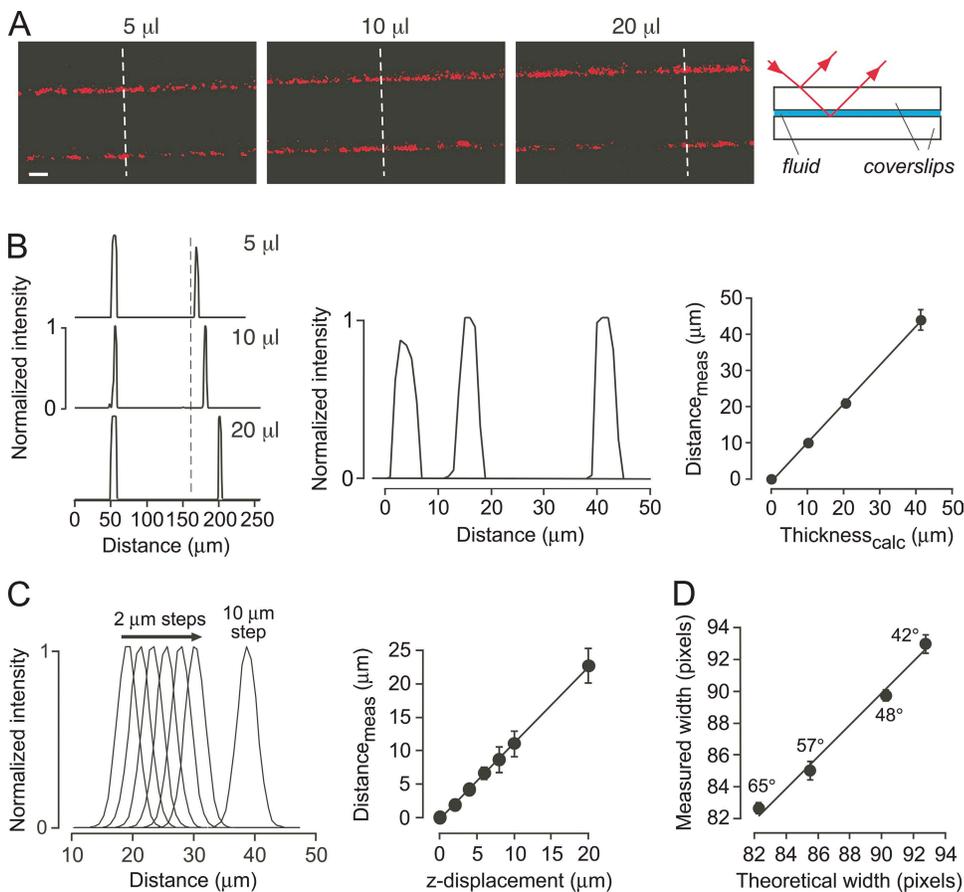
Figure 2. Surface reflectance validation and resolution. (A) SLRM images of fluid layers (volumes, 5, 10, and 20 µl) sandwiched between cover glasses. (Right) Schematic showing origin of the reflections. (B; left) Corresponding intensity versus distance profiles measured at dashed white lines in A. (Middle) Distance-expanded view of second reflections. (Right) Fluid thickness computed from fluid volume added (Thickness$_{calc}$) as a function of fluid thickness measured by SLRM (Distance$_{meas}$). Mean ± SEM of five measurements per cover glass with linear regression ($r^2 = 0.99$). (C; left) Intensity versus distance profiles for reflections from a cover glass, with 2-µm displacements in the z-direction. (Right) Corresponding computed displacements (Distance$_{meas}$) against actual z-displacement. Mean ± SEM of five measurements. (D) Measured width in pixels (8× magnification) between reflections for a 100-µm-thick cover glass as a function of incident light angle versus theoretical width calculated from incident light angle, and cover glass thickness (78 pixels) and refractive index. Mean ± SEM of three measurements.

junctions. The suitability of cell culture inserts for reflectance imaging was first tested using cell culture inserts without cells. Due to surface tension effects between the plastic sidewalls of the insert and the deposited fluids, which produces a meniscus, relatively large volumes (100–300 µl) of fluid were used to cover the entire area of the porous filter. Fig. 3 A shows increasing fluid depths result in increased displacement of reflections from the air–liquid and liquid–filter interfaces. Confocal z-scans of equivalent, fluorescently stained fluid layers confirmed the accuracy of the SLRM measurements (Fig. 3 B). The meniscus effect is responsible for the nonlinear relation between added fluid volume and fluid layer thickness. Fig. 3 C shows an SLRM image of two fluid layers on a cell culture insert (oil and PBS), with the resulting intensity profile showing distinct peaks corresponding to each interface.

ASL depth in well-differentiated HBE cell cultures

Having validated the SLRM method using model fluid layers, measurements of ASL depth were done on well-differentiated HBE cells grown on cell culture inserts. To compare measurements made by SLRM against those made by z-scanning fluorescence confocal microscopy, initial experiments were performed using standard protocols for ASL depth measurement involving washing the mucosal surface and the addition of small amounts of fluorescently stained buffer, and making measurements after a steady-state ASL depth was achieved. Fig. 4 A (left) shows representative SLRM images at three locations in a bronchial cell culture after a steady-state ASL depth was achieved, with associated intensity versus distance profiles shown on the right. Dashed lines indicate reflections from the ASL surface. Fig. 4 A (right) shows a confocal z-scan from the same cell insert, with associated z-intensity profile and histogram analysis of ASL depths over the full imaged area. ASL depth as measured by SLRM was 8.8 ± 0.2 µm, in agreement with ASL depth measured by confocal microscopy on the same cells (8.4 ± 1.0 µm), and in agreement with many prior studies (Tarran et al., 2001; Song et al., 2009).

The dynamics of ASL depth after the addition of fluid to the mucosal surface was followed using SLRM, with confocal microscopy measurements done in parallel. Fig. 4 B shows that ASL depth was reduced over 6 h until a steady-state ASL was achieved as a consequence of fluid absorption. Good agreement was found between SLRM and confocal measurements. The addition of 100 µM amiloride to the mucosal solution reduced the rate of fluid absorption.
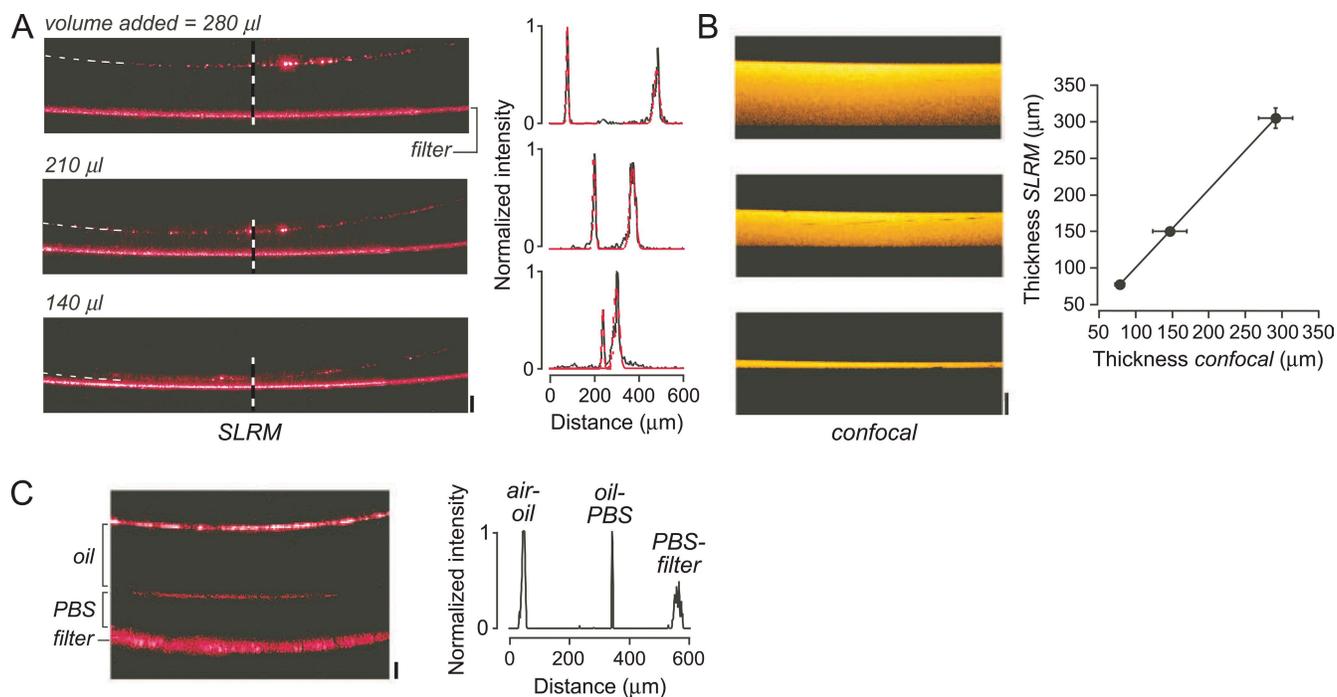
Figure 3. Surface reflections from fluid layer and cell culture insert interfaces. (A; left) SLRM images of a polycarbonate cell culture insert containing different volumes (140, 210, and 280 µl) of deposited PBS. Top reflection corresponds to air–liquid interface and bottom reflection to liquid–filter interface. Bar, 100 µm. Horizontal width of image is 2.5 mm. (Right) Corresponding intensity versus distance profiles (black) at locations of dashed vertical lines, with fitted Gaussians (red). (B; left) Corresponding confocal z-scans. Bar, 100 µm. Horizontal width is 236 µm. (Right) Fluid layer thickness measured by SLRM against that measured by z-scanning confocal microscopy. Mean ± SEM of three measurements ($r^2 = 0.99$). (C; left) SLRM image of oil layer above PBS fluid layer on a polycarbonate insert. Bar, 100 µm. (Right) Corresponding intensity versus distance profile.

ASL depth in "native" cultures was also measured by SLRM using unperturbed bronchial cell cultures that were not subjected to washing or the addition of buffer to the mucosal surface. The SLRM image in Fig. 4 C shows areas of increased ASL depth, which were found in all cultures studied. ASL depth was in the range of 7–20 µm, with an average of 11.3 ± 3.7 µm. A representative surface plot of ASL depth in Fig. 4 D shows considerable heterogeneity, with several areas having depth >10 µm. Fig. 4 E summarizes ASL depth values measured by SLRM.

ASL depth in ex vivo porcine airways

SLRM was also used to measure ASL depth in ex vivo fragments of pig trachea. With a similar protocol to that used in the cell cultures, a small volume (20 µl) of PBS containing dye was added to the mucosal surface, with SLRM and confocal measurements of ASL depth made over 8 h. Fig. 5 A (left) shows good mapping of the surface contours of the mucosa and the overlying fluid layer by SLRM. Associated intensity versus distance plots show decreasing ASL depth over time. There was marked heterogeneity in the depth of the fluid layer, depending on whether the laser line was positioned over a relatively raised or depressed section of the mucosa. Heterogeneity was seen as well in confocal z-scans (Fig. 5 A, middle), albeit dependent on the exact position of the objective. To quantify fluid absorption, an average ASL depth was calculated for several tracheal fragments. Fig. 5 A (right) shows gradual reduction in ASL depth over 6–8 h, with ASL depth becoming more homogenous across the mucosal surface. This change from a relatively heterogeneous to homogenous ASL thickness is shown by a number histogram analysis of measurements across a single culture, with reduced spread of measured depths at 8 h versus earlier times. Fig. 5 B shows SLRM and confocal images of ASL depth after stimulation with a combination of secretory agonists (forskolin plus IBMX plus carbachol). ASL depth increased slowly after agonist stimulation as measured by SLRM.

Transepithelial water permeability

SLRM was applied to measure transepithelial water permeability in human bronchial cell cultures from the kinetics of fluid layer thickness after an osmotic challenge.
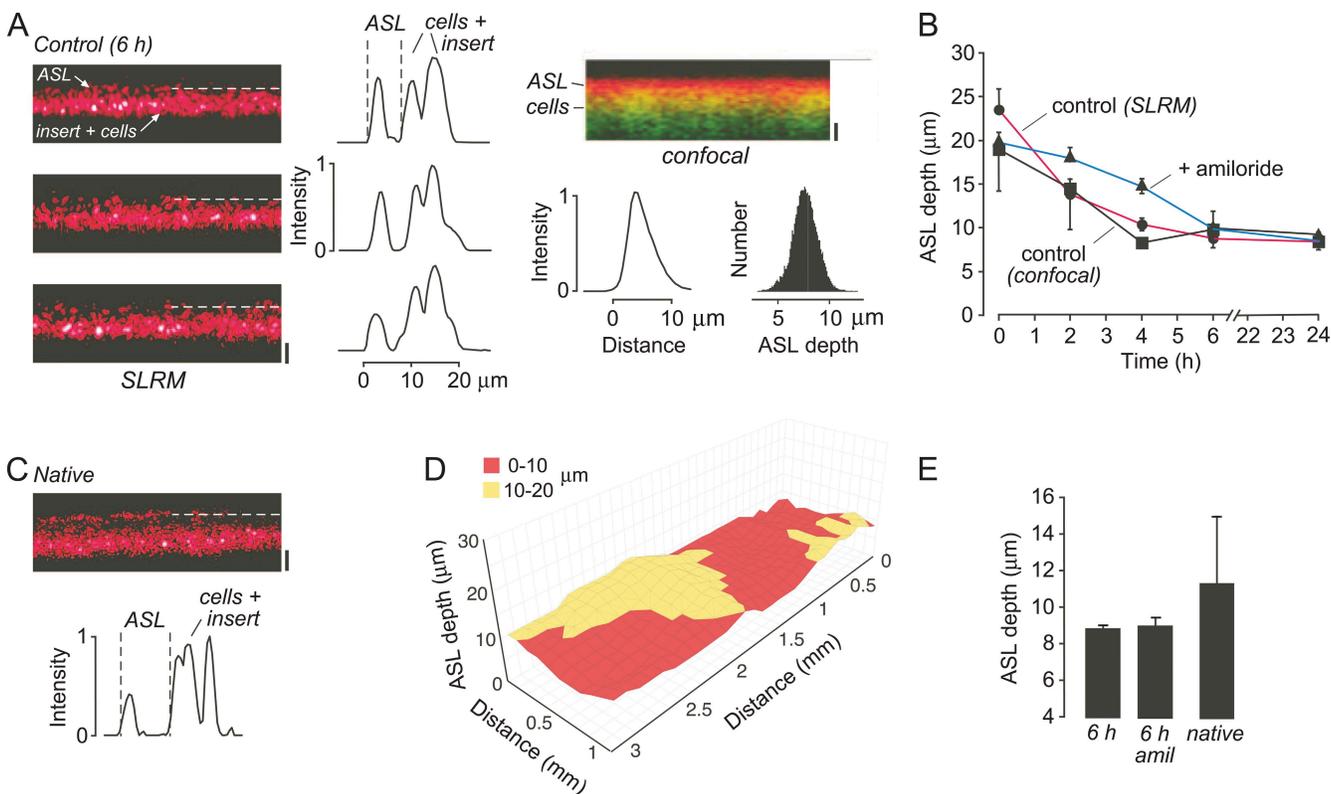
Figure 4. ASL measurements in well-differentiated HBE cell cultures. (A; left) SLRM images of ASL at three locations in an HBE culture 6 h after rinsing and the addition of 20 µl buffer. Dashed line indicates ASL surface. Bar, 10 µm. (Middle) Corresponding intensity versus distance profiles perpendicular to laser line. (Right) Confocal imaging showing ASL (red) and epithelium (green) under same conditions as in A. Bar, 10 µm. Corresponding fluorescence z-profile and ASL depth number histogram shown below image. (B) Time course of ASL depth after the addition of 20 µl buffer in untreated HBE cells measured by SLRM (circles, red lines) and z-scanning confocal microscopy (squares), and by SLRM after treatment with 100 µM amiloride. Mean ± SEM of three cell inserts. (C) SLRM image of unperturbed native ASL from HBE cells, with corresponding intensity profile shown below. Bar, 10 µm. (D) Surface plot of ASL depth in native HBE cells. (E) Summary of ASL depths measured by SLRM. Mean ± SEM of three cell inserts.

Fig. 6 A shows the reduced mucosal fluid layer height over time after the addition of a hyperosmolar solution to the basolateral perfusate, resulting in osmotic water flow as indicated. Fluid height changed linearly over the first 10 min after a small initial lag that is probably related to slow access of fluid to the basolateral cell surface across the porous insert. Fluid height was stable in the absence of an osmotic gradient (not depicted). The computed osmotic water permeability coefficient (P_f) was 48 ± 7 µm/s. P_f in T84 cells was found to be slightly lower, 33 ± 1 µm/s. Reversal of the osmotic gradient in the bronchial cells using a hypoosmolar solution (Fig. 6 B) gave a P_f of 42 ± 8 µm/s.

DISCUSSION

SLRM allowed accurate measurement of ASL depth without the need for staining of the ASL with fluorescent dyes or covering the ASL with nonaqueous fluid. SLRM does not require scanning confocal microscopy, using instead a simple, inexpensive optical system

consisting of a line laser source, focusing optics, and camera detector. Validation studies indicated micronresolution accuracy for measurement of fluid layer thickness. SLRM was applied in well-differentiated bronchial epithelial cell cultures and intact ex vivo airway fragments for measurement of absolute ASL depth and changes in ASL depth in response to active fluid absorption/secretion and imposed osmotic gradients. The simplicity of the SLRM method should allow its wide use for studies of ASL regulation, as well as investigation of the utility of ASL depth measurement as a surrogate endpoint to evaluate ion channel–targeted CF therapies.

The technical requirements for ASL depth measurement by SLRM include precise spatial localization of laser reflections and imaging of both specular and diffuse interfacial reflections. Spatial localization was afforded by the use of a micro-focus diode laser, which produced a narrow line of 13-µm width. The narrow beam profile and sharp edge, with 25–75% intensity change over 300 nm, afforded submicron spatial resolution. Also, the elongated beam profile allowed imaging of ASL in
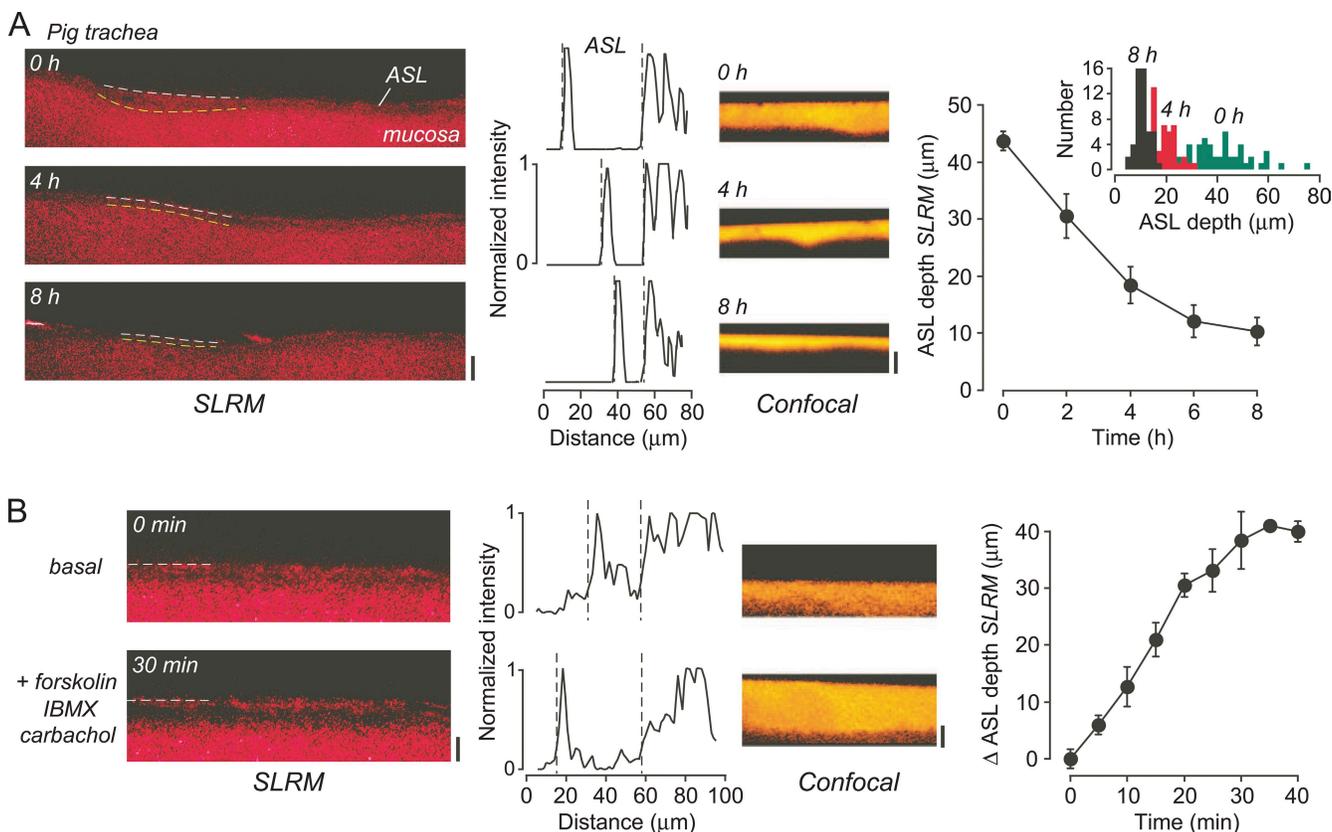
Figure 5. ASL measurements in pig trachea. (A; left) SLRM images at indicated times after the addition of 20 µl PBS containing rhodamine B-dextran. Bar, 40 µm. (Middle left) Corresponding intensity versus distance profiles perpendicular to laser line. (Middle right) Corresponding confocal z-scans. Bar, 40 µm. (Right) Time course of ASL depth after the addition of 20 µl PBS containing rhodamine B-dextran. Mean ± SEM of three tracheal fragments. (Inset) Histogram of ASL depths from 50 measurements across SLRM image at indicated times. (B; left) SLRM images before and 30 min after the addition to the perfusate of 20 µM forskolin, 100 µM IBMX, and 1 mM carbachol. Bar, 40 µm. (Middle left) Corresponding intensity versus distance profiles perpendicular to laser line. (Middle right) Corresponding confocal z-scans. Bar, 40 µm. (Right) Time course of ASL depth after the addition of agonists. Mean ± SEM of three tracheal fragments. SLRM images were contrast-adjusted to obtain sharpest intensity versus distance profiles.
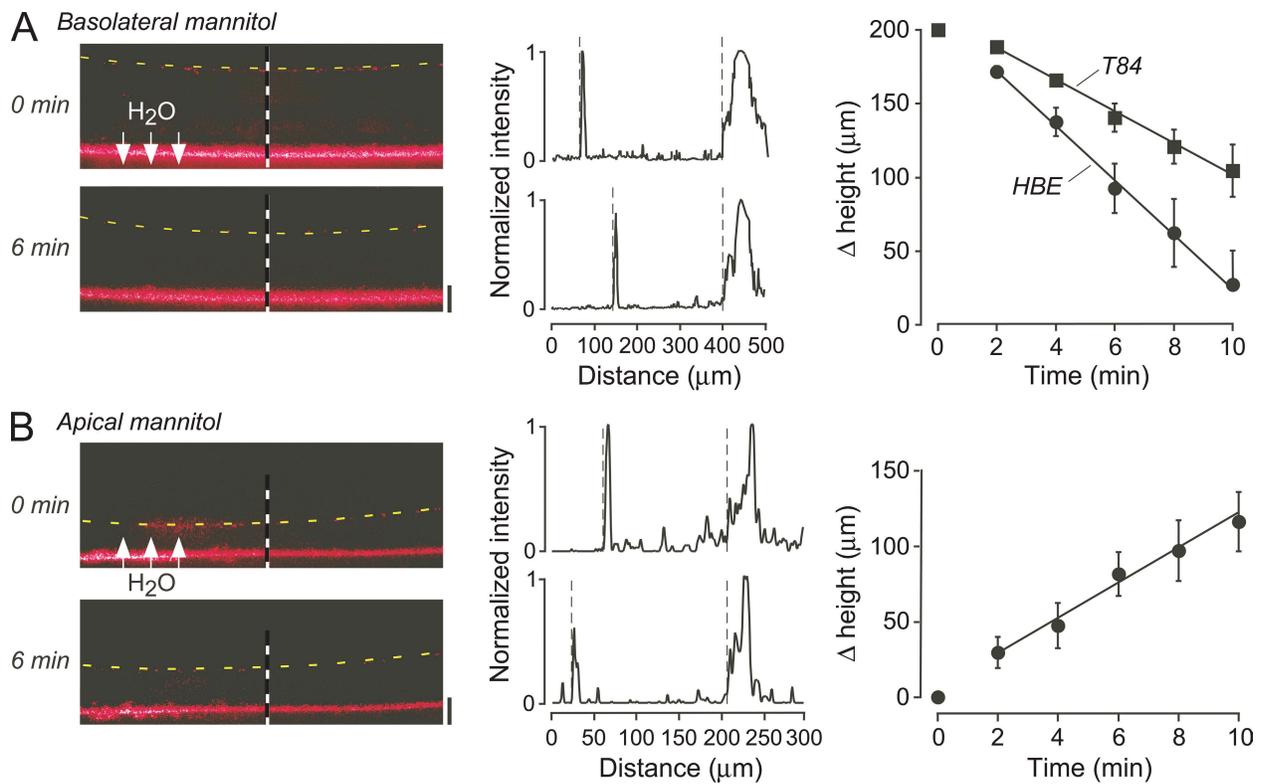
Figure 6. Transepithelial water permeability. (A; left) SLRM images of HBE cells before and 6 min after the addition of 300 mM mannitol to the basolateral perfusate. Dashed lines indicates fluid surface. (Middle) Corresponding intensity versus distance profiles shown at locations of dashed vertical lines. (Right) Time course of change in fluid height in HBE and T84 cells. Mean ± SEM of three cell inserts. (B; left) SLRM images before and 6 min after the addition of 300 mM mannitol to apical fluid in HBE cells. (Middle) Corresponding intensity versus distance profiles. (Right) Time course of change in fluid height. Mean ± SEM of three cell inserts.

the illuminated region from a single image acquired in <500 ms, thereby allowing detection of rapid changes in ASL and cell thicknesses. Imaging of specular and diffuse interfacial reflections was afforded by using an objective lens with broad depth of focus, as used in inexpensive dissecting microscopes.

There are several limitations of SLRM as currently configured. The micro-focus laser used here is well-suited for measurement of fluid layer thicknesses of tens of microns, as the line width remains small (13–20 µm) over these distances. However, due to the focusing optics in the laser, there is a distance dependence (depth of field) of the line width that results in substantially larger line widths at distances >100 µm away from the focal plane, which limits the resolution in measuring thick (>50-µm) fluid layers. Use of alternative laser focusing methods or stage z-repositioning would allow accurate micron-resolution measurement of greater fluid layer thicknesses. Another optical issue is the meniscus effect caused by nonaqueous fluids above the ASL, such as perfluorocarbon, as sometimes used to prevent ASL evaporation and as an immersion fluid for an objective lens in confocal microscopy. The meniscus effect at the edges causes spherical aberration of the incident laser light and consequent blurring at the line edge, which, in the

current optical configuration, prevents accurate fluid thickness measurements across the whole width of the cell monolayer. Last, the use of standard cell culture inserts, without additional optics such as mirrors or prisms, precludes shallow illumination angles because of the height of side walls.

In addition to the general optical limitations, there are some specific issues related to measuring ASL in cell monolayers. First, the scattering/reflective properties of turbid media such as the ASL confers diffuse laser light reflections from the air–liquid interface, instead of the largely specular reflections in simple fluid layers such as saline or oil. Also, the scattering properties of single-cell monolayers, cultured on inserts, make it difficult to distinguish between reflections from the surface of cells and the underlying membrane. These issues are of lesser concern in measurements in tissues, such as ex vivo tracheal fragments, as the reflections arising from the mucosal surface are quite distinct and easily resolvable. The ASL boundary was also occasionally blurred due to movement of cilia. Last, although our interface detection algorithm using a simple Gaussian regression gave consistent results that were validated empirically, improved resolution might be afforded by the use of more sophisticated boundary edge detection algorithms.

SLRM was applied to measure ASL depth in well-differentiated HBE cell cultures grown at an air–liquid interface, as studied in many prior reports. The measurements were made initially using a standard protocol for measuring ASL depth involving washing of the mucosal surface, the addition of buffer containing dye, and measuring ASL depth after multi-hour incubation to achieve a stable, steady-state ASL depth. The ASL depth measured using SLRM agreed well with that measured in parallel by confocal z-scanning microscopy. ASL depth was also measured by SLRM in the studies here without perturbation of the ASL by washing or fluid additions. In contrast to the quite homogenous ASL depth found using the standard washing equilibration protocol, the ASL depth in unperturbed cultures was heterogeneous across the surface of the cells, varying by as much as 10 μm. The ASL consists of two distinct layers: a mucus layer overlying a liquid periciliary or "sol" layer (Lucas and Douglas, 1934; Yoneda, 1976; Lillehoj and Kim, 2002). Measurements of ASL depth by SLRM or confocal microscopy do not distinguish between these two layers. This uncertainty is generally avoided in studies of ASL depth regulation by removing the mucus layer and allowing a largely liquid layer to develop on the mucosal surface. Differences in the effects of ion channel inhibitors/activators such as amiloride have been previously suggested to be due to variability in cell culture preparation and ASL staining (Tarran et al., 2001; Song et al., 2009). The increased ASL depth in native unperturbed ASL found here is likely due to the presence of a heterogenous mucus layer. It should be noted that the cultures of HBE cells used here were well differentiated with relatively low mucus secretion. It may be informative to measure ASL depth by SLRM in cultures more representative of the composition of the native airway mucosa that include mucus-secreting goblet cells. Interestingly, prior studies have shown important regulatory effects of the mucus on dynamics of ASL regulation (Lillehoj and Kim, 2002; Tarran, 2004), and, given recent data suggesting an important but as yet undefined role for CFTR in mucus production (Garcia et al., 2009; Yu et al., 2010), this topic warrants further investigation.

In addition to experiments in cell culture, the SLRM method was used to measure ASL depth in intact ex vivo fragments of pig trachea. The SLRM method worked well in these experiments, giving easily distinguishable interface edges. SLRM allowed mapping of the surface contours of the mucosa, which allows more accurate determination of ASL depth across the whole surface area. Another advantage of SLRM over existing methods is the ability to rapidly measure dynamic changes in ASL depth, as can occur during agonist- and osmotic-driven transepithelial absorption and secretion.

The SLRM method developed here has some similarities to Brewster angle microscopy as used in materials science to investigate ultrathin films (<10 nm) on air–water interfaces or on dielectric substrates (Winsel et al., 2003; McGillivray et al., 2009). In Brewster angle microscopy, there is no reflectance for an air–water interface or dielectric substrate for vertically linearly polarized light at the Brewster angle of incidence. Overlying thin film layers can be distinguished by small increases in reflectance caused by the change of refractive index. This method is particularly good at distinguishing lipid/surfactant layers above homogenous fluid–solid interfaces with high resolution; however, the underlying fluid layer is invisible. The SLRM method represents an adaptation of this basic principle (albeit at much lower resolution) in which the nonpolarized reflections from layers of different refractive indices are imaged. Other methods for visualizing thin layers include interferometry with incident light of various wavelengths (Ghim and Kim, 2006). Interferometry methods have nanometer resolution but are not useful in measuring micron-thick fluid layers such as the ASL, and would be overly sensitive to the airway cell surface irregularities and airway ciliary movement. A recent high-resolution method to image airways in vivo and in vitro is anatomical optical coherence tomography (aOCT). This method is able to resolve airway structure and diameter, and has been recently used to measure airway lumen narrowing in response to stimulants (Noble et al., 2010). The aOCT method is based on interferometry of infrared light and therefore allows high-contrast imaging of the airway mucosal surface. However, aOCT does not resolve the airway fluid layer above the mucosal surface. aOCT may be a useful adjunct to SLRM in vivo using fiberoptics for simultaneous imaging of the airway surface and the overlying surface liquid.

Adaptations of the SLRM method introduced here should allow for: (a) 3-D imaging of the ASL and cell surface; (b) simultaneous determination of ASL thickness and composition; and (c) in vivo fiberoptic measurement of ASL thickness. Sample scanning by stage displacement in a direction perpendicular to the long axis of the laser spot gives a series of slices through the ASL, which, when assembled side by side, yields a 3-D replica of the ASL/cell surface. Simultaneous recording of the 670-nm laser reflection image with fluorescence images of one or more dyes in the ASL or cell cytoplasm should allow for simultaneous determination of ASL/cell thickness and compositional parameters such as pH, $[Na^+]$, $[K^+]$, and $[Cl^-]$, each of which is measurable using ratioable fluorescent dyes (Jayaraman et al., 2001; Namkung et al., 2009). Although the measurements here were done using a distinct laser source and a commercial stereozoom dissecting microscope and CCD camera, the required optics, comprising a laser spot/line source and a focused camera detector, are adaptable to fiberoptic instrumentation for endoscopic measurements in live large animals, such as pigs, as well as in human subjects.

In conclusion, we have developed and validated a new method for measuring small fluid layers such as the ASL that requires minimal perturbation. SLRM should allow for more widespread investigation of the dynamics of ASL depth regulation in cell cultures and tissues, and perhaps in vivo.

REFERENCES

Blouquit-Laye, S., and T. Chinet. 2007. Ion and liquid transport across the bronchiolar epithelium. *Respir. Physiol. Neurobiol.* 159:278–282. doi:10.1016/j.resp.2007.03.007

Boucher, R.C. 2004. Relationship of airway epithelial ion transport to chronic bronchitis. *Proc. Am. Thorac. Soc.* 1:66–70. doi:10.1513/pats.2306018

Boucher, R.C. 2007. Airway surface dehydration in cystic fibrosis: pathogenesis and therapy. *Annu. Rev. Med.* 58:157–170. doi:10.1146/annurev.med.58.071905.105316

Garcia, M.A., N. Yang, and P.M. Quinton. 2009. Normal mouse intestinal mucus release requires cystic fibrosis transmembrane regulator-dependent bicarbonate secretion. *J. Clin. Invest.* 119: 2613–2622. doi:10.1172/JCI38662

Ghim, Y.S., and S.W. Kim. 2006. Thin-film thickness profile and its refractive index measurements by dispersive white-light interferometry. *Opt. Express.* 14:11885–11891. doi:10.1364/OE.14.011885

Jayaraman, S., Y. Song, L. Vetrivel, L. Shankar, and A.S. Verkman. 2001. Noninvasive in vivo fluorescence measurement of airway-surface liquid depth, salt concentration, and pH. *J. Clin. Invest.* 107:317–324. doi:10.1172/JCI11154

Kreindler, J.L. 2010. Cystic fibrosis: exploiting its genetic basis in the hunt for new therapies. *Pharmacol. Ther.* 125:219–229. doi:10.1016/j.pharmthera.2009.10.006

Lillehoj, E.R., and K.C. Kim. 2002. Airway mucus: its components and function. *Arch. Pharm. Res.* 25:770–780. doi:10.1007/BF02976990

Lucas, A.M., and L.C. Douglas. 1934. Principles underlying ciliary activity in the respiratory tract. II. A comparison of nasal clearance in man, monkey, and other mammals. *Arch. Otolaryngol.* 20:518–541.

McGillivray, D.J., J.P. Mata, J.W. White, and J. Zank. 2009. Nano- and microstructure of air/oil/water interfaces. *Langmuir.* 25:4065–4069. doi:10.1021/la802865z

Nakagami, Y., S. Favoreto Jr., G. Zhen, S.W. Park, L.T. Nguyenvu, D.A. Kuperman, G.M. Dolganov, X. Huang, H.A. Boushey, P.C. Avila, and D.J. Erle. 2008. The epithelial anion transporter pendrin is induced by allergy and rhinovirus infection, regulates airway surface liquid, and increases airway reactivity and inflammation in an asthma model. *J. Immunol.* 181:2203–2210.

Namkung, W., Y. Song, A.D. Mills, P. Padmawar, W.E. Finkbeiner, and A.S. Verkman. 2009. In situ measurement of airway surface liquid [K$^+$] using a ratioable K$^+$-sensitive fluorescent dye. *J. Biol. Chem.* 284:15916–15926. doi:10.1074/jbc.M808021200

Noble, P.B., A.R. West, R.A. McLaughlin, J.J. Armstrong, S. Becker, P.K. McFawn, J.P. Williamson, P.R. Eastwood, D.R. Hillman, D.D. Sampson, and H.W. Mitchell. 2010. Airway narrowing assessed by anatomical optical coherence tomography in vitro: dynamic airway wall morphology and function. *J. Appl. Physiol.* 108:401–411. doi:10.1152/japplphysiol.00511.2009

Rahmoune, H., and K.L. Shephard. 1995. State of airway surface liquid on guinea pig trachea. *J. Appl. Physiol.* 78:2020–2024.

Song, Y., W. Namkung, D.W. Nielson, J.W. Lee, W.E. Finkbeiner, and A.S. Verkman. 2009. Airway surface liquid depth measured in ex vivo fragments of pig and human trachea: dependence on Na$^+$ and Cl$^-$ channel function. *Am. J. Physiol. Lung Cell. Mol. Physiol.* 297:L1131–L1140. doi:10.1152/ajplung.00085.2009

Tarran, R. 2004. Regulation of airway surface liquid volume and mucus transport by active ion transport. *Proc. Am. Thorac. Soc.* 1:42–46. doi:10.1513/pats.2306014

Tarran, R., B.R. Grubb, J.T. Gatzy, C.W. Davis, and R.C. Boucher. 2001. The relative roles of passive surface forces and active ion transport in the modulation of airway surface liquid volume and composition. *J. Gen. Physiol.* 118:223–236. doi:10.1085/jgp .118.2.223

Thelin, W.R., and R.C. Boucher. 2007. The epithelium as a target for therapy in cystic fibrosis. *Curr. Opin. Pharmacol.* 7:290–295. doi:10.1016/j.coph.2007.01.004

Verkman, A.S., Y. Song, and J.R. Thiagarajah. 2003. Role of airway surface liquid and submucosal glands in cystic fibrosis lung disease. *Am. J. Physiol. Cell Physiol.* 284:C2–C15.

Winsel, K., D. Hönig, K. Lunkenheimer, K. Geggel, and C. Witt. 2003. Quantitative Brewster angle microscopy of the surface film of human broncho-alveolar lavage fluid. *Eur. Biophys. J.* 32:544–552. doi:10.1007/s00249-003-0290-2

Wu, D.X., C.Y. Lee, J.H. Widdicombe, and J. Bastacky. 1996. Ultrastructure of tracheal surface liquid: low-temperature scanning electron microscopy. *Scanning.* 18:589–592. doi:10.1002/sca .4950180809

Yager, D., T. Cloutier, H. Feldman, J. Bastacky, J.M. Drazen, and R.D. Kamm. 1994. Airway surface liquid thickness as a function of lung volume in small airways of the guinea pig. *J. Appl. Physiol.* 77:2333–2340.

Yoneda, K. 1976. Mucous blanket of rat bronchus: an ultrastructural study. *Am. Rev. Respir. Dis.* 114:837–842.

Yu, K., R. Lujan, A. Marmorstein, S. Gabriel, and H.C. Hartzell. 2010. Bestrophin-2 mediates bicarbonate transport by goblet cells in mouse colon. *J. Clin. Invest.* 120:1722–1735.